

Metallic surface electronic state in half-Heusler compounds $RPtBi$ ($R = Lu, Dy, Gd$)

Chang Liu,^{1,2} Yongbin Lee,¹ Takeshi Kondo,^{1,2} Eun Deok Mun,^{1,2} Malinda Caudle,^{1,2}
Bruce N. Harmon,^{1,2} Sergey L. Bud'ko,^{1,2} Paul C. Canfield,^{1,2} and Adam Kaminski^{1,2}

¹*Division of Materials Science and Engineering, Ames Laboratory, Ames, Iowa 50011, USA*

²*Department of Physics and Astronomy, Iowa State University, Ames, Iowa 50011, USA*

(Dated: January 7, 2011)

Rare-earth platinum bismuth ($RPtBi$) has been recently proposed to be a potential topological insulator. In this paper we present measurements of the metallic surface electronic structure in three members of this family, using angle resolved photoemission spectroscopy (ARPES). Our data shows clear spin-orbit splitting of the surface bands and the Kramers' degeneracy of spins at the $\bar{\Gamma}$ and \bar{M} points, which is nicely reproduced with our full-potential augmented plane wave calculation for a surface electronic state. No direct indication of topologically non-trivial behavior is detected, except for a weak Fermi crossing detected in close vicinity to the $\bar{\Gamma}$ point, making the total number of Fermi crossings odd. In the surface band calculation, however, this crossing is explained by another Kramers' pair where the two splitting bands are very close to each other. The classification of this family of materials as topological insulators remains an open question.

I. INTRODUCTION

The discovery of topologically non-trivial states of matter opens up a new realm of knowledge for fundamental condensed matter physics. Unlike conventional materials, these "topological insulators" exhibit metallic surface states that are protected by time reversal symmetry, while maintaining an insulating bulk electronic structure. This leads to a variety of novel properties including odd number of surface Dirac fermions, strict prohibition of back-scattering, etc., paving the way to potential technical breakthroughs in e.g. quantum computing process via the application of spintronics^{1,2}. Recently, extensive theoretical and experimental efforts have led to the realization of such fascinating behaviors in e.g. the HgTe quantum wells³⁻⁵, the $Bi_{1-x}Sb_x$ system⁶⁻⁸ and the Bi_2X_3 ($X = Te, Se$) binary compounds^{9,10}. Numerous half-Heusler ternary compounds have been proposed, theoretically, to be potential new platforms for topological quantum phenomena^{11,12}, where the inherent flexibility of crystallographic, electronic and superconducting parameters provide a multidimensional basis for both scientific and technical exploration. The experimental determination of their topological class would set the basis for possible spintronic utilization and further studies on the interplay between the topological quantum phenomena versus e.g. the magnetic¹³, superconducting¹⁴ and heavy Fermionic¹⁵ behaviors.

Theoretically, the topological insulators experience a gapless surface state protected by time reversal symmetry and thus are robust against scattering from local impurities. Such a surface state is "one half" of a normal metal in that the surface bands are strongly spin-polarized, forming a unique spin helical texture^{7,16}. On the other hand, the Kramers' theorem requires that the spin be degenerate at the Kramers' points - k -points of the surface Brillouin zone where time reversal symmetry is preserved¹⁷. At the interface between, say, a normal spin-orbit system and vacuum, the spin-polarized sur-

face bands connect pairwise (Kramers' pair), crossing the chemical potential μ an even number of times between two distinct Kramers' points. At the interface between a topologically non-trivial material and vacuum, however, one expects the surface bands to cross μ an odd number of times¹.

In this paper we present a systematic survey on the surface electronic structure of half-Heusler compounds $RPtBi$ ($R = Lu, Dy, Gd$) using angle resolved photoemission spectroscopy (ARPES). Our results show clear spin-orbit splitting of the surface bands that cross the chemical potential, which is nicely reproduced in the full-potential augmented plane wave calculation for a surface electronic state. The Kramers' degeneracy of spin is unambiguously detected at both the $\bar{\Gamma}$ and \bar{M} points. No direct indication of topologically non-trivial behavior is detected, except for the fact that there is a weak Fermi crossing in the close vicinity to the $\bar{\Gamma}$ point, making the total number of crossings five. In the surface band calculation, however, this inner crossing is explained by two spin-orbit splitting bands that are very close to each other, forming another Kramers' pair. In this band configuration, the total Berry phase would be zero for the half-Heusler systems, and they would not be topologically non-trivial. The detailed topological class of this family of materials thus remains an open question, requiring a detailed spin-resolved ARPES study with ultra-high momentum resolution and a direct calculation of the topological invariants based on the first principle band structure.

II. EXPERIMENTAL

Single crystals of $RPtBi$ ($R = Lu, Dy, Gd$) were grown out of a Bi flux and characterized by room temperature power X-ray diffraction measurements^{13,18}. The crystals grow as partial octahedra with the (111) facets exposed. Typical dimensions of a single crystal are about $0.5 \times 0.5 \times 0.5$ mm³. The ARPES measurements were

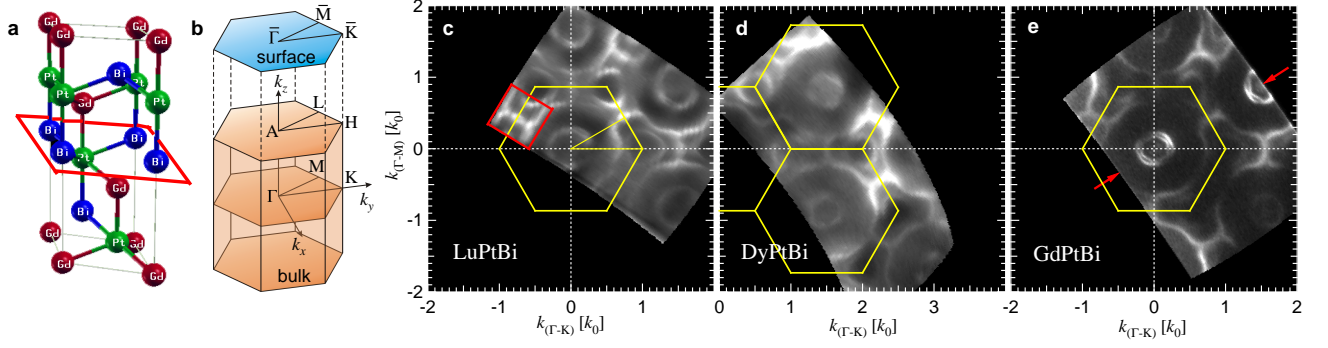


FIG. 1: (Color online) Surface Fermi maps of half-Heusler compounds $RPtBi$ ($R = \text{Lu, Dy, Gd}$). (a) $C1_b$ Crystal structure of $RPtBi$. The crystallographic axes are rotated so that the (111) direction points along z . The red parallelogram marks the Bi(111) cleaving plane. (b) The surface and bulk Brillouin zone for the rotated crystal structure in (a). Here k_z corresponds to the (111) direction of the fcc Brillouin zone. (c)-(e) Surface Fermi maps of $RPtBi$. All data is taken with 48 eV photons at $T = 15$ K. Yellow lines denote the surface Brillouin zone.

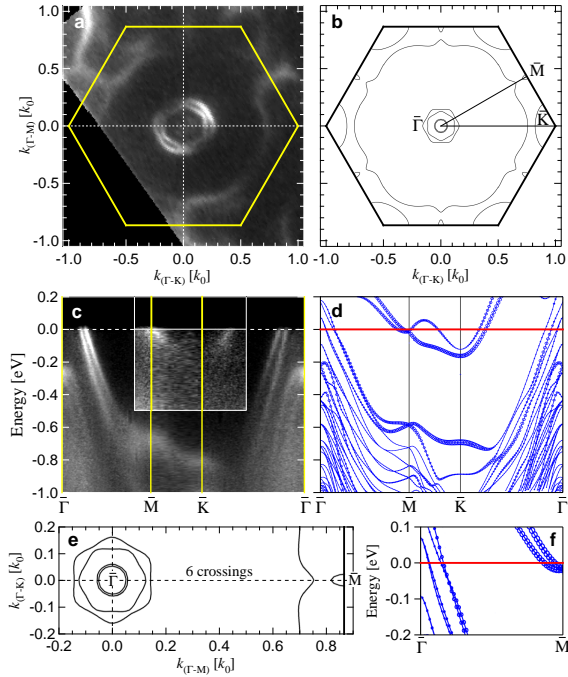


FIG. 2: (Color online) Surface electronic structure of GdPtBi: Comparison between ARPES data and calculational result. (a) Fermi map of GdPtBi observed by ARPES, same as Fig. 1(e). (b) Calculational surface Fermi map of GdPtBi at the Bi(111) cleaving plane. See text for details. (c) ARPES band structure along the contour $\bar{\Gamma}-\bar{M}-\bar{K}-\bar{\Gamma}$. Inset of (c) enhanced the ARPES intensity near \bar{M} and \bar{K} for better visibility of the bands. (d) Calculational band structure with respect to (c). (e)-(f) Expanded figures for (b) and (d), respectively, showing six Fermi crossings. Panel (e) is rotated by 30° with respect to (b).

performed at beamline 10.0.1 of the Advanced Light Source (ALS), Berkeley, California using a Scienta R4000 electron analyzer. Vacuum conditions were better than

3×10^{-11} torr. All ARPES data was taken at $T = 15$ K, above the magnetic ordering temperatures of all compounds¹³. The energy resolution was set at ~ 15 meV. All samples were cleaved *in situ*, yielding clean (111) surfaces in which atoms arrange in a hexagonal lattice. High symmetry points for the surface Brillouin zone are defined as $\bar{\Gamma}(0,0)$, $\bar{K}(k_0,0)$ and $\bar{M}(0,k_0\sqrt{3}/2)$ with unit momentum $k_0 = \sqrt{6}\pi/a$, where a is the lattice constant for each type of crystals. We emphasize here that no stress or pulling force is felt by the samples, which ensures that the measured data reveals the intrinsic electronic structure of the single crystals.

III. RESULTS AND DISCUSSION

We begin this survey in Fig. 1 by showing the Fermi maps of the three half-Heusler compounds $RPtBi$ ($R = \text{Lu, Dy, Gd}$). Previous theoretical calculations for the bulk electronic structure^{11,12,19} suggested that the Kramers' crossing at the $\bar{\Gamma}$ point happens very close to μ ; the Fermi surface reduces to a single point (Dirac point) at $\bar{\Gamma}$. The data in Fig. 1 shows that, at least in the (111) cleaving plane, this is not the case. Instead there are several bands crossing μ in the vicinity of both the $\bar{\Gamma}$ and \bar{M} points. The overall Fermi surface for all three half-Heusler compounds are similar, indicating a similar cleaving plane and band structure for all members. By comparing the band structure measured at the (111) surface with results of band calculations for GdPtBi (Fig. 2), we find the cleaving plane to be Bi(111), marked by a red parallelogram in Fig. 1(a). A closer look at Fig. 1(c)-(e) reveals that the $\bar{\Gamma}$ pockets have different sizes for different Heusler members. For example the circular $\bar{\Gamma}$ pockets in LuPtBi are larger in size than those in GdPtBi. This indicates a different effective electron occupancy for different members of the half-Heusler family. One should also note that in Fig. 1(e) the inner of

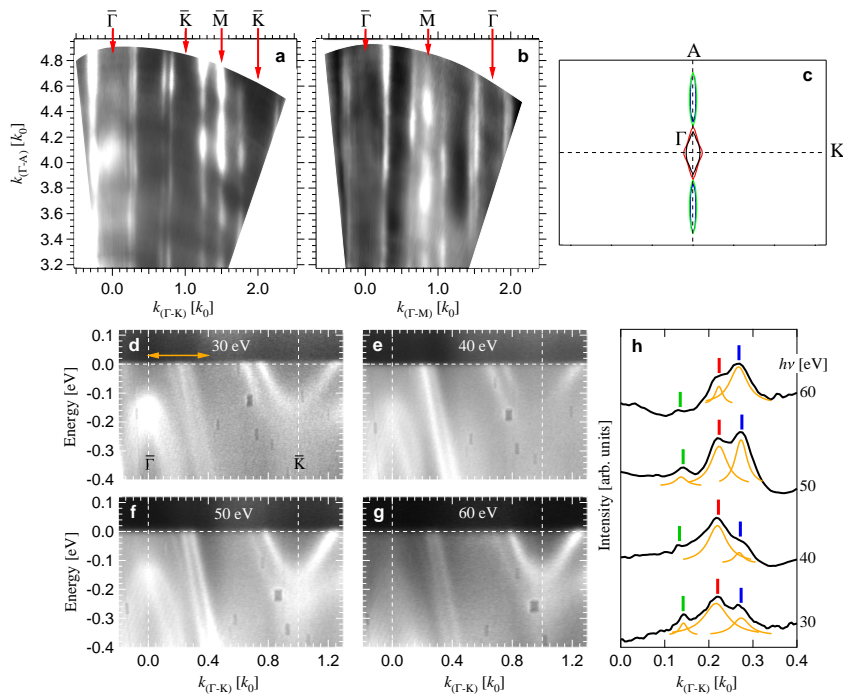


FIG. 3: (Color online) Absence of k_z dispersion as proof for the observation of a surface electronic structure. (a)-(b) k_z (Γ-A) dispersion maps for LuPtBi. Data is obtained by scanning the incident photon energy $h\nu$ from 30 to 80 eV along (a), the $\bar{\Gamma}$ - \bar{K} and (b) the $\bar{\Gamma}$ - \bar{M} direction. (c) Calculational Fermi surface map for the *bulk* state in the A-Γ-K plane. See panel (a) for comparison. (d)-(g) Band dispersion maps along the $\bar{\Gamma}$ - \bar{K} direction for selected $h\nu$ s. It is clear that all observed bands are independent of $h\nu$ (k_z). (h) Detailed peak analysis for the momentum distribution curves (MDCs) at the chemical potential for four different photon energies. k range is indicated by an orange double arrow in (d). Bars in different colors indicate the Fermi crossings for different bands.

the two bright $\bar{\Gamma}$ pockets is hexagonal in shape, reminiscent of the hexagonal shape of the Dirac cone in Bi_2Te_3 (Ref.¹⁰), which is explained by higher order terms in the $k \cdot p$ Hamiltonian²⁰. This hexagonal shape is very nicely reproduced in the calculation [Fig. 2(b)]. For clarifying the topological class of the half-Heuslers, two immediate questions follow the observations in Fig. 1: (1) Are the observed bands actually arising due to the sample surface? (2) Exactly how many times do the bands intersect the chemical potential along the $\bar{\Gamma}$ - \bar{M} line segment?

Fig. 2 shows the comparison between the ARPES data and a calculational surface state in GdPtBi. For both the band structure and Fermi surface calculation, we used a full-potential linear augmented plane wave (FPLAPW) method²¹ with a local density functional²². The crystallographic unit cell is generated such that the (111) direction of the *fcc* Brillouin zone points along the z -axis. For calculation of the surface electronic structure, supercells with three unit cell layers and a 21.87 a.u. vacuum is constructed. We calculated band structures of all six possible surface endings (Gd-Bi-Pt-bulk, Gd-Pt-Bi-bulk, Bi-Gd-Pt-bulk, Bi-Pt-Gd-bulk, Pt-Gd-Bi-bulk, Pt-Bi-Gd-bulk); only the Bi-Pt-Gd-bulk construction shows good agreement with experiment [Fig. 2(b), (d)-(f)]. Structural data were taken from a reported experimental result²³. To obtain the self-consistent charge density, we chose 48 k -points in the irreducible Brillouin zone, and set $R_{\text{MT}} \times k_{\text{max}}$ to 7.5, where R_{MT} is the smallest muffin-tin radius and k_{max} is the plane-wave cutoff. We used muffin-tin radii of 2.5, 2.4 and 2.4 a.u. for Gd, Bi, and Pt respectively. For the non-magnetic-state calculation valid for comparison with ARPES results at 15 K, the seven 4*f* electrons of Gd atoms were treated as core electrons with no net spin polarization. The atoms

near the surface (Bi, Pt, Gd) were relaxed along the z -direction until the forces exerted on the atoms were less than 2.0 mRy/a.u.. With this optimized structure, we obtained self-consistency with 0.01 mRy/cell total energy convergence. After that, we calculated the band structure and two dimensional Fermi surface in which we divided the rectangular cell connecting four \bar{K} -points by 40×40 , yielding 1681 k -points.

Even at first glance, Fig. 2 gives the impression of remarkable agreement between theory and experiment. All basic features observed by ARPES - the overall shape and location of the Fermi pockets [Fig. 2(a)-(b)], the binding energies of the bands [Fig. 2(c)-(d)] - are well reproduced by the calculation. The main point of this figure, however, is the fact that band calculations show a total of six Fermi crossings along the $\bar{\Gamma}$ - \bar{M} line segment, which is an even number and is not directly consistent of the proposed strong topological insulating phenomenon^{11,12}. It should be noted that, in order to take into account the spin-orbit splitting, relativistic effects are applied to the calculation. Similar calculations reproduce clear topological insulating behavior in Bi_2Te_3 thin films²⁴. The excellent agreement shown in Fig. 2 also implies the validity of such calculation in half-Heusler compounds. In fact traces for the inner two crossings is also found in the ARPES data, where they appear to be one single crossing, most likely due to finite momentum resolution [Leftmost part in Fig. 2(c), see also Fig. 3(d)-(h)].

In Fig. 3 we prove that the observed bands come from the sample surface. This is done by scanning the incident photon energy along both $\bar{\Gamma}$ - \bar{K} and $\bar{\Gamma}$ - \bar{M} high symmetry directions. Varying the photon energy in ARPES effectively changes the momentum offset along the direction perpendicular to the sample surface. In our case, this

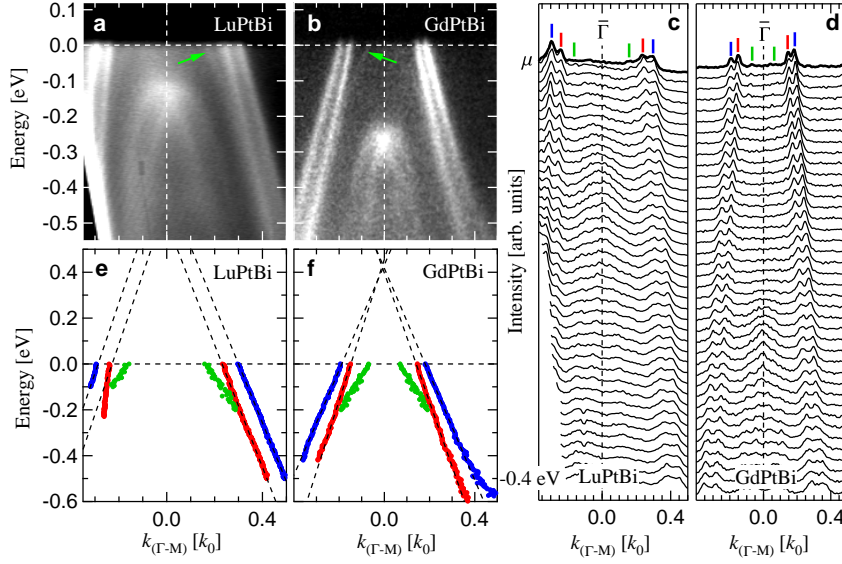


FIG. 4: Band structure analysis at the vicinity of $\bar{\Gamma}$ [red arrows in Fig. 1(e)]. Data is taken on LuPtBi and GdPtBi samples at $T = 15$ K. (a)-(b) Band dispersion maps along the $\bar{\Gamma}$ - \bar{M} direction. Green arrows point to the position of the inner hole band which have lower intensity than the two other hole bands. (c)-(d) Corresponding MDCs for panels (a) and (b). (e)-(f) Extraction of the band position for panels (a) and (b). By linearly extrapolating the bands above the chemical potential μ we show an approximate band crossing point (Dirac point) at $E \sim 0.4$ eV for GdPtBi.

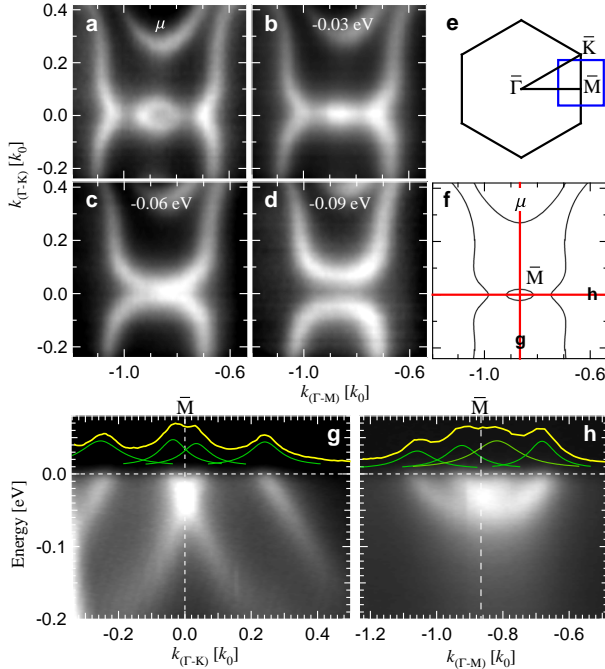


FIG. 5: Band structure analysis at the vicinity of \bar{M} [red box in Fig. 1(c)]. Data is taken on LuPtBi samples. (a)-(d) Binding energy dependence of band structure near \bar{M} . Map location in the surface Brillouin zone is shown in Panel (e). (f) Theoretical band map at the chemical potential for GdPtBi. (g),(h) Band maps for two perpendicular directions marked by red lines in (g). There are in total two Fermi crossings along the $\bar{\Gamma}$ - \bar{M} line segment at the vicinity of \bar{M} .

direction corresponds to k_z or the (111) direction of the *fcc* Brillouin zone. Figs. 3(a)-(b) show that all observed bands form straight lines along the k_z direction, a clear indication for the lack of k_z dependence. In Fig. 3(c) we

compare this to a calculated Fermi surface map for the *bulk* bands, along the same direction as in Fig. 3(a). The difference is clear: the bulk bands are dispersive along the $\bar{\Gamma}$ - \bar{A} direction; and most of the experimentally observed bands are not present in the calculation. In Figs. 3(d)-(h) we pay special attention to the bands crossing μ near $\bar{\Gamma}$ by showing the band structure for four different photon energies. In total there are at least three Fermi contours surrounding $\bar{\Gamma}$, the outer two being a lot brighter than the inner one (or two, see discussion for Fig. 2). As shown in Fig. 3(h), These three (or four) bands cross μ at exactly the same k positions for all photon energies. Therefore all of them are surface bands. The data in Fig. 3 thus show, unambiguously, that a metallic surface electronic state exists in the half-Heusler compounds.

The exact number of Fermi crossings along the $\bar{\Gamma}$ - \bar{M} line segment is also examined in Fig. 4. The main conclusion for Fig. 4 is that there are also three (or four) visible Fermi crossings at the vicinity of $\bar{\Gamma}$ between these two Kramers' points. We show these bands on the LuPtBi and GdPtBi samples. Both on the band dispersion maps [Figs. 4(a)-(b)] and the momentum distribution curves [MDCs, Figs. 4(c)-(d)] we see that there are two bright hole-like bands almost parallel to each other, and a much weaker inner band with lower Fermi velocity. This inner band is not easy to see in the band maps (nonetheless indicated by green arrows), but is clearly visible in the MDCs by small intensity peaks tracing down from the one marked by a green bar [also marked by a green color in Figs. 4(e)-(f)]. The same band also exists in the $\bar{\Gamma}$ - \bar{K} direction [Figs. 3(d)-(h)]. Same as the discussion for Figs. 2 and 3, this inner crossing is reproduced in the band calculation by two closely located spin-orbit-splitting bands that form a Kramers' pair. The brighter parallel bands form a second Kramers' pair of opposite spins. In Fig. 4(e)-(f) we show the linear extrapolation of the two brighter bands. In GdPtBi they are likely to

reduce to a Dirac point at about 0.4 eV above μ . If the total number of crossing is four, such a configuration will give zero contribution to the total Berry phase.

In Fig. 5 we examine the bands near the \bar{M} point. The k -space location of the ARPES maps [Figs. 5(a)-(d)] is shown in Fig. 5(e). Panels 5(g)-(h) present the band dispersion maps for two cuts crossing \bar{M} , whose positions are marked in Panel 5(f) with the band calculation result. Figs. 5(a)-(d) show that the \bar{M} bands form a very special shape. At high binding energies [$E \sim -0.1$ eV, Fig. 5(d)], two U-shape bands are well separated. As binding energy decreases these two bands merge into each other and hybridize to form a central elliptical contour and two curly-bracket-like segments. The segments near each \bar{M} points link together, forming another large Fermi contour enclosing the zone center $\bar{\Gamma}$. It is clear from Fig. 5(g)-(h) that there are two Fermi crossings in both the $\bar{\Gamma}$ - \bar{K} and $\bar{\Gamma}$ - \bar{M} directions. The special shape of the Fermi surface is formed by two bands that are likely to be members of another Kramers' pair. Kramers' degeneracy of spin happens at ~ 30 meV below μ . All this features are obtained with our calculation for the surface states [Fig 2(b) and 2(e)]. These two bands also give zero contribution to the total Berry phase.

In summary, we performed an ARPES survey on the electronic structure of three half-Heusler compounds $RPtBi$ ($R = \text{Lu, Dy, Gd}$) which are proposed to be topo-

logical insulators. Our result show unambiguously that these materials have a metallic surface state markedly different from the calculational result on the bulk electronic structures. This surface state is reproduced with high accuracy in our band calculations. Both experiment and theory reveal several bands that cross the Fermi level. Knowledge of the exact number of these bands is possibly limited by experimental momentum resolution. No direct consistency with the proposed strong topological insulating behavior is found in the ARPES results. For final determination of their topological classes, both an APRES measurement of ultrahigh k -resolution and a direct calculation of the first Chern number as a topological invariant²⁵ are in need.

IV. ACKNOWLEDGEMENT

We thank S.-C. Zhang and J. Schmalian for instructive discussions as well as Sung-Kwan Mo for grateful instrumental support at the ALS. Ames Laboratory was supported by the Department of Energy - Basic Energy Sciences under Contract No. DE-AC02-07CH11358. ALS is operated by the US DOE under Contract No. DE-AC03-76SF00098.

-
- ¹ M. Z. Hasan and C. L. Kane, Rev. Mod. Phys. **82**, 3045 (2010).
 - ² J. E. Moore, Nature (London) **464**, 194 (2010).
 - ³ B. A. Bernevig, T. L. Hughes, and S.-C. Zhang, Science **314**, 1757 (2006).
 - ⁴ M. König, S. Wiedmann, C. Brüne, A. Roth, H. Buhmann, L. W. Molenkamp, X.-L. Qi, and S.-C. Zhang, Science **318**, 766 (2007).
 - ⁵ A. Roth, C. Brüne, H. Buhmann, L. W. Molenkamp, J. Maciejko, X.-L. Qi, and S.-C. Zhang, Science **325**, 294 (2009).
 - ⁶ D. Hsieh, D. Qian, L. Wray, Y. Xia, Y. S. Hor, R. J. Cava, and M. Z. Hasan, Nature (London) **452**, 970 (2008).
 - ⁷ D. Hsieh, Y. Xia, L. Wray, D. Qian, A. Pal, J. H. Dil, J. Osterwalder, F. Meier, G. Bihlmayer, C. L. Kane, Y. S. Hor, R. J. Cava, and M. Z. Hasan, Science **323**, 919 (2009).
 - ⁸ P. Roushan, J. Seo, C. V. Parker, Y. S. Hor, D. Hsieh, D. Qian, A. Richardella, M. Z. Hasan, R. J. Cava, and A. Yazdani, Nature (London) **460**, 1106 (2009).
 - ⁹ H. Zhang, C.-X. Liu, X.-L. Qi, X. Dai, Z. Fang, S.-C. Zhang, Nature Physics **5**, 438 (2009).
 - ¹⁰ Y. L. Chen, J. G. Analytis, J.-H. Chu, Z. K. Liu, S.-K. Mo, X. L. Qi, H. J. Zhang, D. H. Lu, X. Dai, Z. Fang, S. C. Zhang, I. R. Fisher, Z. Hussain, and Z.-X. Shen, Science **325**, 178 (2009).
 - ¹¹ S. Chadov, X.-L. Qi, J. Kübler, G. H. Fecher, C. Felser, and S.-C. Zhang, Nature Materials **9**, 541 (2010).
 - ¹² H. Lin, L. A. Wray, Y. Xia, S. Xu, S. Jia, R. J. Cava, A. Bansil, and M. Z. Hasan, Nature Materials **9**, 546 (2010).
 - ¹³ P. C. Canfield, J. D. Thompson, W. P. Beyermann, A. Lacerda, M. F. Hundley, E. Peterson, Z. Fisk, and H. R. Ott, J. Appl. Phys. **70**, 5800 (1991).
 - ¹⁴ G. Goll, M. Marz, A. Hamann, T. Tomanic, K. Grube, T. Yoshino, and T. Takabatake Physica B **403**, 1065 (2008).
 - ¹⁵ Z. Fisk, P. C. Canfield, W. P. Beyermann, J. D. Thompson, M. F. Hundley, H. R. Ott, E. Felder, M. B. Maple, M. A. Lopez de la Torre, P. Visani, and C. L. Seaman, Phys. Rev. Lett. **67**, 3310 (1991).
 - ¹⁶ D. Hsieh, Y. Xia, D. Qian, L. Wray, J. H. Dil, F. Meier, J. Osterwalder, L. Patthey, J. G. Checkelsky, N. P. Ong, A. V. Fedorov, H. Lin, A. Bansil, D. Grauer, Y. S. Hor, R. J. Cava and M. Z. Hasan, Nature (London) **460**, 1101 (2009).
 - ¹⁷ C. L. Kane and E. J. Mele, Phys. Rev. Lett. **95**, 146802 (2005).
 - ¹⁸ P. C. Canfield and Z. Fisk, Philos. Mag. B **65**, 1117 (1992).
 - ¹⁹ V. N. Antonov, P. M. Oppeneer, A. N. Yaresko, A. Y. Perlov, and T. Kraft, Phys. Rev. B **56**, 13012 (1997).
 - ²⁰ L. Fu, Phys. Rev. Lett. **103**, 266801 (2009).
 - ²¹ P. Blaha, K. Schwarz, G. K. H. Madsen, D. Kvasnick and J. Luitz, WIEN2k, An augmented plane wave plus local orbitals program for calculation crystal properties (K. Schwarz, TU wien, Austria, 2001) ISBN 3-9501031-1-2.
 - ²² J. P. Perdew and Y. Wang, Phys. Rev. B **45**, 13244 (1992).
 - ²³ M. G. Haase, T. Schmit, C. G. Richter, H. Block, and W. Jeitschko, J. Solid State Chem. **168**, 18 (2002).
 - ²⁴ K. Park, J. J. Heremans, V. W. Scarola, and D. Minic, arXiv:1005.3476 (unpublished) (2010).
 - ²⁵ X.-L. Qi, T. L. Hughes, and S.-C. Zhang, Phys. Rev. B **78**,

195424 (2008) and references therein.